Hall-on-Toric State: Descendant Laughlin State in the Chiral $\mathbb{Z}_p$ Toric Code

Robin Schäfer,[1,2,3] Claudio Chamon,[4,5] and Chris R. Laumann[1,6]

[1]*Department of Physics, Boston University, Boston, Massachusetts 02215, USA*
[2]*Helmholtz-Zentrum Berlin für Materialien und Energie, Hahn-Meitner-Platz 1, 14109 Berlin, Germany*
[3]*Dahlem Center for Complex Quantum Systems and Fachbereich Physik, Freie Universität Berlin, Arnimallee 14, 14195 Berlin, Germany*
[4]*Department of Physics and Astronomy, Purdue University, West Lafayette, Indiana, 47907*
[5]*Purdue Quantum Science and Engineering Institute, Purdue University, West Lafayette, Indiana, 47907*
[6]*Max-Planck-Institut für Physik komplexer Systeme, 01187 Dresden, Germany*

(Received 31 July 2025; revised 24 February 2026; accepted 11 March 2026; published 22 April 2026)

We demonstrate that the chiral $\mathbb{Z}_p$ toric code—the quintessential model of topological order—hosts additional, emergent topological phases when perturbed: descendant fractional quantum Hall-like states, which we term *Hall-on-Toric*. These hierarchical states feature fractionalized $\mathbb{Z}_p$ charges and increased topological ground-state degeneracy. The Hall-on-Toric phases appear in the vicinity of the transitions between deconfined $\mathbb{Z}_p$ phases with different background charge per unit cell, in a fixed nontrivial flux background. We confirm their existence through extensive infinite density matrix renormalization group (iDMRG) simulations, analyzing the topological entanglement entropy, entanglement spectra, and a generalized Hall conductance. Remarkably, the Hall-on-Toric states remain robust even in the absence of $U(1)$ symmetry. Our findings reinforce the foundational interpretation of star and plaquette defects as magnetic and electric excitations, and reveal that this perspective extends to a much deeper level.

DOI: 10.1103/f63q-vqz3

In what sense are the emergent electric charges in a toric code like familiar electrons? For example, in a magnetic field due to a background of emergent magnetic charges, would they undergo cyclotron motion? If one could engineer a large "density" of the charges, would further interactions then produce quantum Hall physics?

Here, by tuning into a regime where the ground state hosts a finite density of electric and magnetic charges, we answer these questions in the affirmative using a surprisingly simple canonical model for topological phases—the $\mathbb{Z}_p$ toric code illustrated in Fig. 1(a) [1–5]. We find a ground state phase in which the emergent electric charges form a $\nu = 1/2$-type Bosonic Laughlin state [6], which we refer to as the Hall-on-Toric state.

A major distinction between the Hall-on-Toric states and the usual fractional quantum Hall (FQH) states [6–11] lies in the role of charge conservation. In the latter, the underlying electronic charge is conserved, and the chiral edges required by the topological order carry dissipationless charge currents. Historically, those currents underlie the discovery of the FQH states in transport experiments [8,12] and remain the most robust signature of the effect. In the Hall-on-Toric state, the underlying charges are only conserved modulo p as they are emergent charges of a $\mathbb{Z}_p$ theory. Chiral edges remain, but they carry only thermal currents.

Just as in the hierarchical constructions of FQH states, the topological order of the Hall-on-Toric state can be understood by assuming the $\mathbb{Z}_p$ charges of the toric code form a Hall state of their own. In the low-energy Chern-Simons description, the $\mathbb{Z}_p$ toric code is described by the Lagrangian

$$\mathcal{L}_{TC} = \frac{p}{2\pi}\epsilon a\partial b, \tag{1}$$

where the a and b $U(1)$ gauge fields couple to the e and m quasiparticles, respectively, and ε is the Levi-Civita symbol. Placing the e quasiparticles in a $\nu = 1/2$ state, one obtains

$$\mathcal{L}_{HoT} = \frac{p}{2\pi}\epsilon a\partial b + \frac{1}{2\pi}\epsilon a\partial c + \frac{2}{4\pi}\epsilon c\partial c,$$

where c is an additional $U(1)$ gauge field whose fluxes represent the e quasiparticles. Consequences that follow include [13–15] (i) the topological degeneracy (on a torus) of $2p^2$; (ii) a chiral central charge $c = 1$, or, equivalently, thermal Hall conductance $\kappa_{xy}/T = (\pi^2 k_b^2/3h)$; and (iii) the existence of a quasiparticle carrying $1/2$ of the toric code $\mathbb{Z}_p$ charge. In particular, as the underlying e is only conserved modulo p, we have that $2p - 1$ of the $e/2$ quasiparticles are equivalent to one quasihole.

These notable long-wavelength consequences only appear provided the topological state *is* stabilized on the lattice. While the Hall-on-Toric states do not appear in the

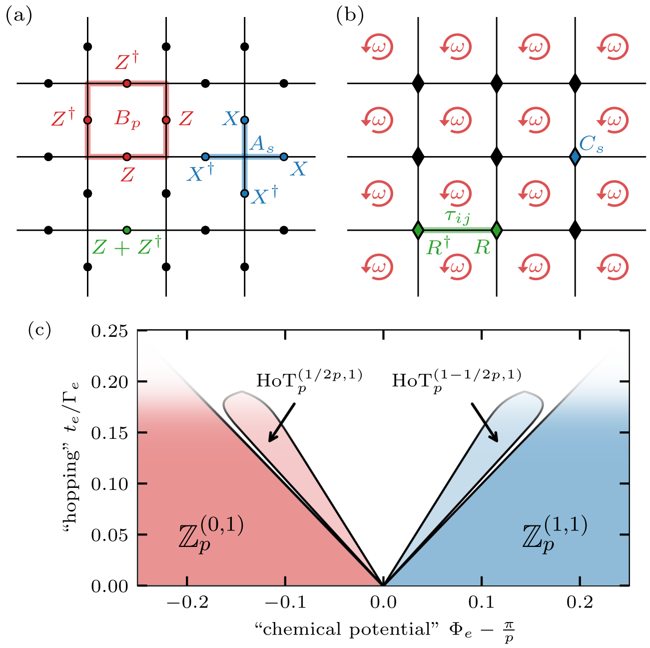

FIG. 1. (a) The $\mathbb{Z}_p$ degrees of freedom of the chiral toric code reside on the edges of the square lattice, Eq. (4). (b) The e and m excitations live on the sites of the lattice and dual, respectively. The e dynamics can be mapped to a pure $\mathbb{Z}_p$ matter model in a fixed background flux $\langle B_p \rangle = \omega$, Eq. (7). (c) Schematic phase diagram illustrating the gapped Hall-on-Toric phases (lobes) in the vicinity of the transition between different background charge states ($\mathbb{Z}_p^{(0,1)}$ and $\mathbb{Z}_p^{(1,1)}$) of the $\mathbb{Z}_p$ theory with fixed background flux. The couplings are defined in Eq. (6) and play the role of $\mathbb{Z}_p$ charge "hopping" and "chemical potential" in the matter model [Eq. (7)].

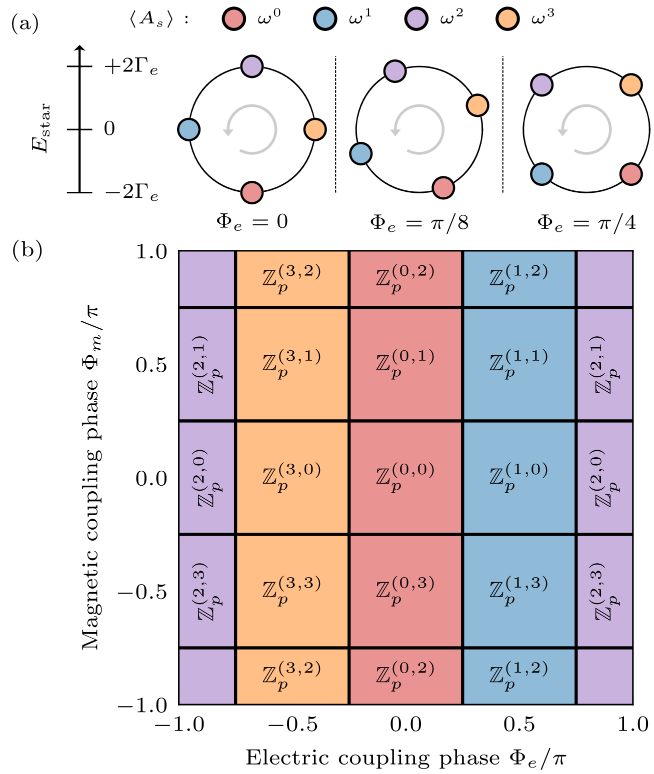

FIG. 2. (a) The spectrum of $e^{-i\Phi_e} A_s + \mathrm{H.c.}$ [see Eq. (5)] can be understood as the height of the p cars (colored eigenstates with eigenvalues the p'th roots of unity) in a Ferris wheel rotated by Φ_e (here, $p = 4$). At $\Phi_e = \pi/4$, a first-order phase transition in the ground state occurs, as the lowest car switches from the red to the blue. (b) Phase diagram of the solvable Hamiltonian H_0 in Eq. (4) ($t_e = 0$). The colors (constant in columns) represent the value of $\langle A_s \rangle$ and refer to the lowest energy state in (a). The value from the plaquette operator $\langle B_p \rangle = \omega^g$ is constant across rows.

phase diagram of the exactly solvable $\mathbb{Z}_p$ toric code model [see Fig. 2(b)], we show that they appear asymptotically close to it in the sense that even weak solvability-breaking perturbations are sufficient. The Hall-on-Toric states intervene near the transitions between $\mathbb{Z}_p$ deconfined phases with different background charge q per unit cell, so long as there is nontrivial background flux g per unit cell to break time reversal symmetry. We denote the reference toric-code phases by $\mathbb{Z}_p^{(q,g)}$ and, following this notation, the descendant Hall-on-Toric phases by $\mathrm{HoT}_p^{(q,g)}$, with q taking fractional values.

Model—The $\mathbb{Z}_p$ generalization of the toric code [16,17] is built from p-dimensional clock degrees of freedom residing on the edges of a square lattice (see Fig. 1(a)) [1–5]. The generalized Pauli operators X and Z are defined with respect to an orthonormal basis $|s\rangle$, $s = 0, \ldots, p-1$,

$$Z|s\rangle = \omega^s |s\rangle \quad \text{and} \quad X|s\rangle = |s - 1 \bmod p\rangle, \tag{2}$$

where $\omega = e^{2\pi i/p}$. The "clock" Z and "shift" X satisfy the generalized commutation relation: $XZ = \omega Z X$. The plaquette and star operators are defined by

$$B_p = \begin{array}{ccc} & Z^\dagger & \\ Z^\dagger & \square & Z \\ & Z & \end{array} \qquad A_s = \begin{array}{ccc} & X & \\ X^\dagger & + & X \\ & X^\dagger & \end{array}. \tag{3}$$

and, just as in the usual toric code, the full set of A_s and B_p operators mutually commute.

The commuting $\mathbb{Z}_p$ toric code Hamiltonian is familiar,

$$H_0 = -\Gamma_m e^{-i\Phi_m} \sum_p B_p - \Gamma_e e^{-i\Phi_e} \sum_s A_s + \mathrm{H.c.} \tag{4}$$

but for the key feature that A_s and B_p are unitary but not Hermitian for $p > 2$. Thus, the couplings can be complex, which we write here in polar form with positive amplitudes, Γ_m and Γ_e, and phases Φ_m and Φ_e. We note that Φ_m is odd under parity and Φ_e is odd under time reversal [18] and thus H_0 defines the *chiral* $\mathbb{Z}_p$ toric code. The sums $\sum_p$ and $\sum_s$ run over all plaquettes and stars, respectively.

As a function of the coupling phases, the Hamiltonian H_0 exhibits p^2 distinct $\mathbb{Z}_p$ deconfined phases, $\mathbb{Z}_p^{(q,g)}$ [see Fig. 2(b)]. Each phase has a topological degeneracy of p^2 on the torus, a topological entanglement entropy of $-\log p$, and host e and m anyons with mutual statistics [1,5,19]. They are distinguished by the background charge q and flux g per unit cell; for the commuting model, these equivalently give the expectation values of the star and plaquette operators in the ground state: $\langle A_s\rangle = \omega^q$ and $\langle B_p\rangle = \omega^g$. For example, the ground state value of $\langle A_s\rangle$ is selected by finding the integer value of q that minimizes

$$E_{\mathrm{star}}(q) = -2\Gamma_e \cos\left(\frac{2\pi q}{p} - \Phi_e\right) \tag{5}$$

for given Φ_e. We illustrate this relation by a rotating clock in Fig. 2(a) showing the energy E_{star} of the $p = 4$ eigenvalues of A_s, which are equidistantly placed on the unit circle. At $\Phi_e = \pi/4$, the system undergoes a first-order transition, where $\langle A_s\rangle$ goes from ω^0 (red) to ω^1 (blue): $\mathbb{Z}_p^{(0,g)} \to \mathbb{Z}_p^{(1,g)}$. An analogous discussion holds for the plaquette operator B_p and the parameter Φ_m.

We perturb the solvable model with a uniform field coupling to Z,

$$H_{\mathrm{TC}} = H_0 - t_e \sum_e (Z_e + Z_e^\dagger). \tag{6}$$

The sum runs over all edges e of the square lattice, and we take the parameter $t_e > 0$ to be real. The full model is illustrated in Fig. 1(a).

Since the perturbation commutes with the plaquette operators B_p, the model remains diagonal in plaquette flux, even as the charges begin to fluctuate. To focus on these dynamics, we extend the Hilbert space by introducing $\mathbb{Z}_p$ matter degrees of freedom, C_s, on the sites of the square lattice, subject to the local Gauss law constraint that $C_s = A_s$ (see supplementary material [18] for more details). In the extended gauge-matter representation, the gauge degrees of freedom are static and we obtain a pure $\mathbb{Z}_p$ matter model,

$$H_{\mathrm{M}} = -\Gamma_e \sum_s e^{-i\Phi_e} C_s - t_e \sum_{\langle i,j\rangle} \tau_{ij} R_i^\dagger R_j + \mathrm{H.c.} \tag{7}$$

Here, R_s is $\mathbb{Z}_p$ conjugate to C_s and τ_{ij} is a fixed gauge background determined by the B_p flux sector of interest. The matter model is a $\mathbb{Z}_p$ version of the Harper-Hofstadter Hamiltonian [20,21]; see Fig. 1(b). We emphasize that Eq. (7) is an exact rewriting of Eq. (6) available so long as the plaquette flux is static.

Consider the transition between two toric code phases $\mathbb{Z}_p^{(0,1)}$ with no background charge per unit cell and $\mathbb{Z}_p^{(1,1)}$ with one background charge per unit cell. At $t_e = 0$, the transition is direct, taking place at $\Phi_e = \pi/p$ where the energy of the two charge states is degenerate as illustrated by the "Ferris wheel" in Fig. 2(a). For $t_e \ll \Gamma_e$, the other charge states are energetically inaccessible and may be projected out. The resulting effective Hamiltonian is a Hofstadter model with hardcore bosons,

$$H_{\mathrm{BH}} = -\mu \sum_s n_s - t_e \sum_{\langle i,j\rangle} \tau_{ij} a_i^\dagger a_j + \mathrm{H.c.} \tag{8}$$

Here, $a_s^\dagger$ and a_s are the bosonic creation and annihilation operators on site s and we have the charge state $C_s = \omega^{n_s}$. The effective chemical potential $\mu = -4\Gamma_e \sin(\pi/p) \sin[(\pi/p) - \Phi_e]$ vanishes at the transition linearly with Φ_e.

In contrast to the unprojected $\mathbb{Z}_p$ model, which only conserves the charge modulo p, the effective bosonic model at small t_e exhibits an emergent $U(1)$ symmetry. Within a Schrieffer-Wolff treatment, virtual processes that eventually break the $U(1)$ are suppressed with $(t_e/\Gamma_e)^{p-1}$ for $p \le 5$. For $p \ge 6$, the suppression becomes even stronger, since additional virtual processes are needed when $p - 1$ exceeds the coordination number of the lattice.

In analogy to the Mott lobes [22] in the Bose-Hubbard problem, we can estimate the splitting of the transition by comparing the single particle energy [20] Δ_p (which is proportional to t_e) with the chemical potential [23]. This gives us the scale, κ_p, on which the toric code phases, $\mathbb{Z}_p^{(0,1)}$ and $\mathbb{Z}_p^{(1,1)}$, give way to intermediate filling,

$$\kappa_p = \arcsin\left(\frac{-\Delta_p}{4\Gamma_e \sin(\pi/p)}\right) \approx \frac{-\Delta_p}{4\Gamma_e \sin(\pi/p)}. \tag{9}$$

The bosonic Hofstadter model has been studied using different numerical methods and found to host a variety of fractional quantum Hall states. It has been explored using exact diagonalization [24–32], DMRG on finite lattices [33,34], iDMRG on cylindrical geometries [31,35,36], tree-tensor networks [37], (i)PEPS [38,39], and various variational and mean-field approaches [24,25,40–42]. While these studies suggest the existence of certain bosonic Hall states—predominantly the bosonic Laughlin state [6] at filling $\nu = 1/2$—the stability of more exotic fractional states in the thermodynamic limit remains uncertain. In particular, topologically trivial density waves and other crystalline states at specific fillings compete with the proposed topologically ordered Hall states. For example, the competition with the Tao-Thouless state [43] has been highlighted in several works [44–46]. This competition is especially relevant in cylindrical geometries, where the circumference becomes comparable to the magnetic unit cell length. Thus, the stability of other filling fractions in the thermodynamic limit remains an open question, as results depend on both the method and system size. Beyond the $\nu = 1/2$ state, some studies [35,36,38] suggest the

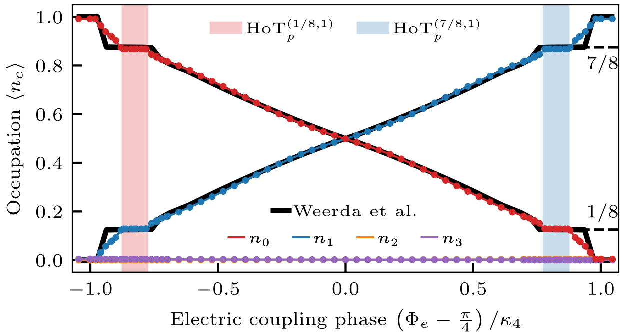

FIG. 3. Charge occupation computed with iDMRG (bond dimension $\chi = 512$) for $p = 4$ and $L_y = 8$, $L_x = 4$ (iDMRG unit cell), and $t_e/\Gamma_e = 0.1$ across the transition at $\Phi_e = \pi/4$ in units of κ_p from Eq. (9). The colors represent the occupation n_c of the individual charge states Eq. (10) within the matter model in Eq. (7) and match Fig. 2. The data in black refers to a number-conserving hardcore bosonic Hofstadter model from Refs. [38,49] (iPEPS). The plateaus correspond to the phases $\mathrm{HoT}_p^{(1/8,1)}$ and $\mathrm{HoT}_p^{(7/8,1)}$.

possibility of a bosonic integer quantum Hall state at $\nu = 2$, which is constructed from composite fermions [27,47]. Given the increased complexity of simulating the $\mathbb{Z}_p$ matter model, we concentrate on the Laughlin state at half filling.

Results—We numerically study the matter model in Eq. (7) with a fixed background flux of $\langle B_p \rangle = \omega$ by placing the system on an infinite cylinder, and computing its ground state using iDMRG [48]. Directly simulating the full toric-code Hamiltonian in Eq. (6) is numerically much more demanding, as it involves twice the number of sites and includes four-body operators. We evaluate the following quantities: (i) $\mathbb{Z}_p$ charge occupation, (ii) topological entanglement entropy, (iii) generalized "Hall conductance," and (iv) the entanglement spectrum.

(i) $\mathbb{Z}_p$ charge occupation: The perturbation t_e splits the first-order transition between the $\mathbb{Z}_p^{(0,1)}$ and $\mathbb{Z}_p^{(1,1)}$ phases and gives rise to a variety of competing phases in between. Figure 3 shows the normalized $\mathbb{Z}_p$ charge occupation for $p = 4$ as a function of Φ_e which refers to a horizontal line cut in Fig. 1(c) at $t_e/\Gamma_e = 0.1$:

$$n_c = \frac{1}{L_x L_y} \sum_s P_{sc}, \tag{10}$$

where P_{sc} is the projector onto the state $|c\rangle$ at site s. The charge occupation n_c is related to the star operator: $A_s = \omega^{q_s}$ with $q_s = \sum_c c P_{sc}$. For comparison, we show data from Refs. [38,49], which have simulated the (hardcore) bosonic Hofstadter model using iPEPS for $p = 4$. Additional data for different p, t_e/Γ_e, and scaling with L_y is shown in Supplemental Material [18].

For $\Phi_e \lesssim (\pi/p) - \kappa_p$, the system is in the $\mathbb{Z}_p^{(0,1)}$ phase, which appears as a trivial paramagnet within the matter model composed solely of red charges with $n_0 = 1$ and zero otherwise. At $\Phi_e \approx (\pi/p) - \frac{5}{6}\kappa_p$, a plateau emerges at fractional charge occupation. The blue charges have increased to a finite density, $n_1 = 1/(2p)$, and form the $\nu = 1/2$ state, embedded in a background of red charges at density, $n_0 = (2p-1)/(2p)$ [50]. We refer to this state as $\mathrm{HoT}_p^{(1/2p,1)}$. An analogous Hall state, $\mathrm{HoT}_p^{(1-1/2p,1)}$, is formed at $\Phi_e \approx (\pi/p) + \frac{5}{6}\kappa_p$, where the roles of the two charge states are reversed. The model exhibits charge-anti-charge symmetry around the transition ($\Phi_e \leftrightarrow 2\pi/p - \Phi_e$), which is composed of charge conjugation and a global charge shift, as defined in the Supplemental Material [18]. This refers to the particle-hole symmetry in the Hofstadter model.

Next, we analyze intrinsic properties of the $\mathrm{HoT}_p^{(1/2p,1)}$ state accessible via its Schmidt decomposition. Thereby, we use the $\mathbb{Z}_p$ symmetry (particle number conservation modulo p) and the translational invariance to group the Schmidt coefficients. k_y refers to the y momentum around the cylinder, and $c = 0, \ldots, p-1$ labels the charge differences across the cut [48,51,52]:

$$|\Psi\rangle = \sum_{k_y} \sum_{c=0}^{p-1} \sum_{i=1}^{\chi(k_y,c)} \Lambda_{(k_y,c,i)} |\psi^L_{(k_y,c,i)}\rangle \otimes |\psi^R_{(k_y,c,i)}\rangle. \tag{11}$$

(ii) Topological entanglement entropy: The first intrinsic property we analyze is the topological entanglement entropy [53,54]. It encodes information about Abelian excitations by extracting a universal correction, γ, to the area law. We compute the entanglement across the cut and obtain γ from the following scaling relation in the matter model:

$$S^{\alpha}_{\mathrm{matter}}(L_y) = c_\alpha L_y + \gamma + \mathcal{O}\left(\frac{1}{L_y}\right). \tag{12}$$

Here, L_y refers to the cylinder's circumference, and α denotes different Rényi entropies. Figure 4 shows the scaling of the von Neumann entropy ($\alpha = 1$) and the second Rényi entropy ($\alpha = 2$) with L_y for different values of p. It shows a good agreement with the expected value of $\gamma = -\log\sqrt{2}$ for $\nu = 1/2$, which remains unchanged across different Rényi entropies [55–58]. We remark that the simulated matter model has frozen out the flux degrees of freedom by employing a fixed gauge. The entanglement entropy in the full $\mathbb{Z}_p$ model includes an additional contribution of $-\log p$ from the gauge sector.

(iii) Generalized "Hall conductance": We further analyze the Hall response by adiabatically threading flux (Θ_y) through the cylinder [7]. This measure is standard for number-conserving systems within iDMRG [36,50,58–61] but we generalized it to the $\mathbb{Z}_p$ case. Using the decomposition of the ground state in Eq. (11), we define the weight per charge channel:

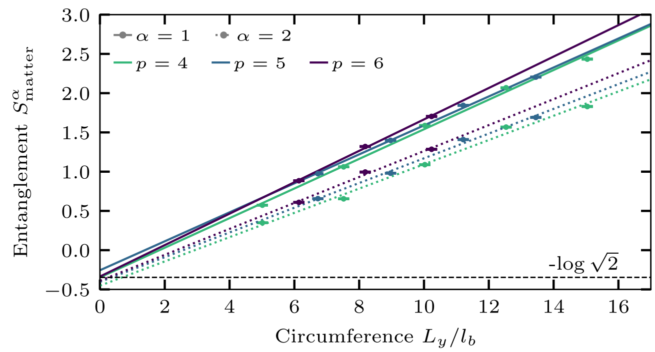

FIG. 4. Topological entanglement entropy of the matter model (Eq. (7) with $t_e/\Gamma_e = 0.05$) ground state measured for different circumferences L_y in units of the magnetic length $l_b = p/2\pi$ along the cut in a cylinder using iDMRG ($\chi \geq 1024$, and $L_x = p$). The black, blue, and red data points correspond to $p = 4$, $p = 5$, and $p = 6$, calculated at $\Phi_e = 0.2368\pi$, $\Phi_e = 0.1825\pi$, and $\Phi_e = 0.1891\pi$, respectively. S_0 and S_1 refer to the von Neumann and first Rényi entropy. The expected topological entanglement entropy of the Hall-on-Toric state is $-\log\sqrt{2}$ (from the Laughlin state) plus the gauge sector contribution $-\log p$.

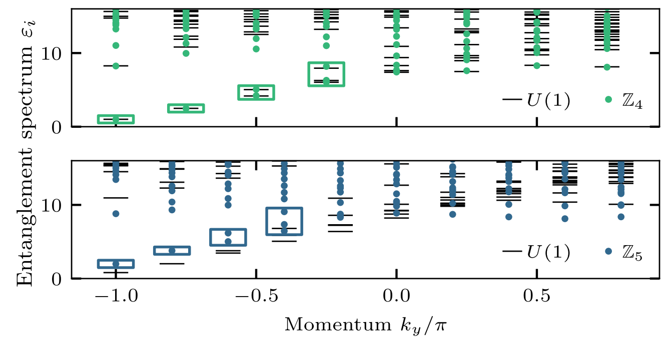

FIG. 5. Entanglement spectrum computed in the matter model [Eq. (7) with $t_e/\Gamma_e = 0.05$] with iDMRG ($\chi = 1024$, $L_x = p$, and $L_y = 2p$) for $p = 4$ ($\Phi_e = 0.2368\pi$) and $p = 5$ ($\Phi_e = 0.1825\pi$) in (a) and (b), respectively. The plots display the entanglement energies $\varepsilon_i = -\log\Lambda_i$ in the $c = 0$ sector, where Λ_i are the Schmidt values obtained from a bipartition along the cylinder. The black stripes indicate the corresponding calculation in the number-conserving Hofstadter model from Eq. (8). The boxes highlight the characteristic counting sequence expected for the Laughlin state.

$$W_c(\Theta_y) \coloneqq \sum_{k_y}\sum_{i=1}^{\chi(k_y,c)} \Lambda^2_{(k_y,c,i)}(\Theta_y). \tag{13}$$

When the system is adiabatically evolved from $\Theta_y = 0$ to $\Theta_y = 4\pi$, we find that the weights shift cyclically:

$$W_c(0) = W_{c+1 \bmod p}(4\pi). \tag{14}$$

In the conventional $U(1)$ case, a similar shift occurs, but without the cyclic constraint. Data and a comparison between the $U(1)$ and $\mathbb{Z}_p$ cases are provided in Supplemental Material [18].

(iv) Entanglement spectrum: The last characteristic we analyze is the entanglement spectrum [62]. For the Laughlin wave function, an edge conformal field theory describing a $U(1)$ chiral Boson predicts a characteristic counting sequence $\{1, 1, 2, 3, \ldots\}$ in the entanglement spectrum, given by $\varepsilon_i = -2\log\Lambda_{(k_y,c,i)}$, when plotted against k_y for each c [36,59,63]. Fig. 5 presents the entanglement spectrum of the matter model Eq. (7) for $p = 4$ and $p = 5$, comparing it with a number-conserving calculation of Eq. (8). While we find excellent agreement for $p = 4$, the $U(1)$ case resolves the sequence more clearly for $p = 5$. We attribute this to the increased computational complexity and anticipate further improvements at higher bond dimensions.

Potential realizations—Recently, $\mathbb{Z}_3$ toric-code order has been demonstrated on a trapped-ion quantum processor with 24 effective qutrits [64]. Per-qutrit fidelities exceeded 95%, and several braiding operations of $\mathbb{Z}_3$ charges were realized. A number of proposals [65] have explored the realization of $\mathbb{Z}_3$-type models across diverse quantum simulation platforms, both predating the trapped-ion experiment and motivated by subsequent developments [66]. While none of these works explicitly target the parameter regime associated with the Hall-on-Toric state, they indicate rapid progress toward a potential experimental realization.

Conclusion—We have demonstrated that the chiral toric code in a small field hosts hierarchical topological states in which the usual deconfined charges form a Laughlin-like Hall state of their own. We refer to these as Hall-on-Toric states. Our understanding is grounded in a perturbative mapping between the $\mathbb{Z}_p$ model and the (number-conserving) bosonic Hofstadter problem. We confirm that the Hall-on-Toric states remain stable even without particle conservation.

Our results are quite surprising, as the Hall-on-Toric state arises in such a small perturbation of a well-known exactly solvable model. On the other hand, this means that the Hall-on-Toric states we find are within sight of well-known bosonic Laughlin states, in which charge nonconservation is only a weak correction to spectral properties. It would be very interesting to find "strong" Hall-on-Toric states which have no analogs in the conventional Hall hierarchies. Such states would presumably take advantage of the modular nature of number conservation in a fundamental way, similarly to the parafermionic states discovered in the context of superconducting proximity effects [67–69]. We leave the search for other Hall-on-Toric states, either weak or strong, to future investigations.

Acknowledgments—R. S. thanks Julian Boesl for insightful discussions. C. R. L. acknowledges the Gutzwiller Fellowship at Max Planck Institute for the Physics of

Complex Systems and the partial support of SFB 1143 and ct.qmat. The work of C. C. is supported by the DOE Grant DE-SC0026189. R. S. was supported by the AFOSR (Grant No. FA9550-24-1-0121). Simulations were conducted using the TENPY package [48].

Data availability—The data used to generate the plots is available on Zenodo [70].

[1] S. S. Bullock and G. K. Brennen, J. Phys. A **40**, 3481 (2007).
[2] M. D. Schulz, S. Dusuel, R. Orús, J. Vidal, and K. P. Schmidt, New J. Phys. **14**, 025005 (2012).
[3] K. Slagle and Y. B. Kim, Phys. Rev. B **96**, 195139 (2017).
[4] S. Vijay, arXiv:1701.00762.
[5] H. Watanabe, M. Cheng, and Y. Fuji, J. Math. Phys. (N.Y.) **64**, 051901 (2023).
[6] R. B. Laughlin, Phys. Rev. Lett. **50**, 1395 (1983).
[7] R. B. Laughlin, Phys. Rev. B **23**, 5632 (1981).
[8] D. C. Tsui, H. L. Stormer, and A. C. Gossard, Phys. Rev. Lett. **48**, 1559 (1982).
[9] F. D. M. Haldane, Phys. Rev. Lett. **51**, 605 (1983).
[10] F. D. M. Haldane, Phys. Rev. Lett. **50**, 1153 (1983).
[11] F. D. M. Haldane, Phys. Rev. Lett. **55**, 2095 (1985).
[12] K. v. Klitzing, G. Dorda, and M. Pepper, Phys. Rev. Lett. **45**, 494 (1980).
[13] X.-G. Wen, *Quantum Field Theory of Many-Body Systems: From the Origin of Sound to an Origin of Light and Electrons* (Oxford University Press, New York, 2007).
[14] E. Fradkin, *Field Theories of Condensed Matter Physics*, 2nd ed. (Cambridge University Press, Cambridge, England, 2013).
[15] S. H. Simon, *Topological Quantum* (Oxford University Press, New York, 2023).
[16] E. Dennis, A. Kitaev, A. Landahl, and J. Preskill, J. Math. Phys. (N.Y.) **43**, 4452 (2002).
[17] A. Y. Kitaev, Ann. Phys. (Amsterdam) **303**, 2 (2003).
[18] See Supplemental Material at http://link.aps.org/supplemental/10.1103/f63q-vqz3 for a detailed description of the model and its gauge representation, along with an analysis of the relevant symmetries. It also includes further results on finite-size scaling and additional parameter regimes, as well as an explanation of the $\mathbb{Z}_p$ Hall conductance.
[19] K. G. Wilson, Phys. Rev. D **10**, 2445 (1974).
[20] P. G. Harper, Proc. Phys. Soc. London Sect. A **68**, 874 (1955).
[21] D. R. Hofstadter, Phys. Rev. B **14**, 2239 (1976).
[22] M. P. A. Fisher, P. B. Weichman, G. Grinstein, and D. S. Fisher, Phys. Rev. B **40**, 546 (1989).
[23] For $p = 4$, the ground-state energy is $\Delta_4 = -2\sqrt{2}$, and we find $\kappa_4 = \arcsin(t_e/\Gamma_e)$.
[24] R. Bai, S. Bandyopadhyay, S. Pal, K. Suthar, and D. Angom, Phys. Rev. A **98**, 023606 (2018).
[25] R. O. Umucalılar and E. J. Mueller, Phys. Rev. A **81**, 053628 (2010).
[26] A. S. Sørensen, E. Demler, and M. D. Lukin, Phys. Rev. Lett. **94**, 086803 (2005).
[27] G. Möller and N. R. Cooper, Phys. Rev. Lett. **103**, 105303 (2009).
[28] M. Hafezi, A. S. Sørensen, E. Demler, and M. D. Lukin, Phys. Rev. A **76**, 023613 (2007).
[29] M. Hafezi, A. S. Sørensen, M. D. Lukin, and E. Demler, Europhys. Lett. **81**, 10005 (2007).
[30] A. Sterdyniak, N. Regnault, and G. Möller, Phys. Rev. B **86**, 165314 (2012).
[31] S. D. Geraedts, C. Repellin, C. Wang, R. S. K. Mong, T. Senthil, and N. Regnault, Phys. Rev. B **96**, 075148 (2017).
[32] T.-S. Zeng, W. Zhu, and D. N. Sheng, Phys. Rev. B **93**, 195121 (2016).
[33] P. Rosson, M. Lubasch, M. Kiffner, and D. Jaksch, Phys. Rev. A **99**, 033603 (2019).
[34] F. A. Palm, M. Buser, J. Léonard, M. Aidelsburger, U. Schollwöck, and F. Grusdt, Phys. Rev. B **103**, L161101 (2021).
[35] Y.-C. He, F. Grusdt, A. Kaufman, M. Greiner, and A. Vishwanath, Phys. Rev. B **96**, 201103(R) (2017).
[36] J. Boesl, R. Dilip, F. Pollmann, and M. Knap, Phys. Rev. B **105**, 075135 (2022).
[37] M. Gerster, M. Rizzi, P. Silvi, M. Dalmonte, and S. Montangero, Phys. Rev. B **96**, 195123 (2017).
[38] E. L. Weerda and M. Rizzi, Phys. Rev. B **109**, L241117 (2024).
[39] E. Macaluso, T. Comparin, R. O. Umucalılar, M. Gerster, S. Montangero, M. Rizzi, and I. Carusotto, Phys. Rev. Res. **2**, 013145 (2020).
[40] D. Hügel, H. U. R. Strand, P. Werner, and L. Pollet, Phys. Rev. B **96**, 054431 (2017).
[41] S. S. Natu, E. J. Mueller, and S. Das Sarma, Phys. Rev. A **93**, 063610 (2016).
[42] E. Ledinauskas and E. Anisimovas, SciPost Phys. **18**, 011 (2025).
[43] R. Tao and D. J. Thouless, Phys. Rev. B **28**, 1142 (1983).
[44] E. H. Rezayi and F. D. M. Haldane, Phys. Rev. B **50**, 17199 (1994).
[45] E. J. Bergholtz, J. Kailasvuori, E. Wikberg, T. H. Hansson, and A. Karlhede, Phys. Rev. B **74**, 081308(R) (2006).
[46] A. Seidel and D.-H. Lee, Phys. Rev. Lett. **97**, 056804 (2006).
[47] J. K. Jain, Phys. Rev. Lett. **63**, 199 (1989).
[48] J. Hauschild and F. Pollmann, SciPost Phys. Lect. Notes 5 (2018).
[49] E. Weerda and M. Rizzi, 10.5281/zenodo.10210305 (2023).
[50] S. D. Huber and N. H. Lindner, Proc. Natl. Acad. Sci. U.S.A. **108**, 19925 (2011).
[51] S. Singh, R. N. C. Pfeifer, and G. Vidal, Phys. Rev. A **82**, 050301(R) (2010).
[52] S. Singh, R. N. C. Pfeifer, and G. Vidal, Phys. Rev. B **83**, 115125 (2011).
[53] M. Levin and X.-G. Wen, Phys. Rev. Lett. **96**, 110405 (2006).
[54] A. Kitaev and J. Preskill, Phys. Rev. Lett. **96**, 110404 (2006).
[55] S. Dong, E. Fradkin, R. G. Leigh, and S. Nowling, J. High Energy Phys. 05 (2008) 016.
[56] Y. Zhang, T. Grover, A. Turner, M. Oshikawa, and A. Vishwanath, Phys. Rev. B **85**, 235151 (2012).
[57] M. P. Zaletel, R. S. K. Mong, and F. Pollmann, Phys. Rev. Lett. **110**, 236801 (2013).
[58] M. P. Zaletel, R. S. K. Mong, and F. Pollmann, J. Stat. Mech. (2014) P10007.

[59] A. G. Grushin, J. Motruk, M. P. Zaletel, and F. Pollmann, Phys. Rev. B **91**, 035136 (2015).
[60] Y.-C. He, D. N. Sheng, and Y. Chen, Phys. Rev. B **89**, 075110 (2014).
[61] Y.-C. He, S. Bhattacharjee, R. Moessner, and F. Pollmann, Phys. Rev. Lett. **115**, 116803 (2015).
[62] H. Li and F. D. M. Haldane, Phys. Rev. Lett. **101**, 010504 (2008).
[63] L. Cincio and G. Vidal, Phys. Rev. Lett. **110**, 067208 (2013).
[64] M. Iqbal, A. Lyons, C. F. B. Lo, N. Tantivasadakarn, J. Dreiling, C. Foltz, T. M. Gatterman, D. Gresh, N. Hewitt, C. A. Holliman, J. Johansen, B. Neyenhuis, Y. Matsuoka, M. Mills, S. A. Moses, P. Siegfried, A. Vishwanath, R. Verresen, and H. Dreyer, Nat. Commun. **16**, 6301 (2025).
[65] G. Giudice, F. M. Surace, H. Pichler, and G. Giudici, Phys. Rev. B **106**, 195155 (2022).
[66] A. Burshtein, S. Fraenkel, M. Goldstein, and R. Finkelstein, Phys. Rev. Res. **8**, 013055 (2026).
[67] N. Read and E. Rezayi, Phys. Rev. B **59**, 8084 (1999).
[68] J. S. Xia, W. Pan, C. L. Vicente, E. D. Adams, N. S. Sullivan, H. L. Stormer, D. C. Tsui, L. N. Pfeiffer, K. W. Baldwin, and K. W. West, Phys. Rev. Lett. **93**, 176809 (2004).
[69] C. Nayak, S. H. Simon, A. Stern, M. Freedman, and S. Das Sarma, Rev. Mod. Phys. **80**, 1083 (2008).
[70] R. Schäfer, C. Chamon, and C. Laumann, Data for “Hall-on-Toric: Descendant Laughlin state in the chiral Zp toric code” (2025), 10.5281/zenodo.16659837.